Environmental Pollution 363 (2024) 125234

Contents lists available at ScienceDirect

Environmental Pollution

journal homepage: www.elsevier.com/locate/envpol

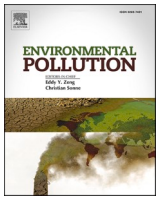

Permeation of per- and polyfluoroalkyl substances (PFAS)-laden leachate in landfills as an outcome of puncture failures of high-density polyethylene geomembranes☆

Simin Moavenzadeh Ghaznavi [a], Anthony Joshue Flores Azua [a], A. Dianne Kopec [b], Luis Zambrano Cruzatty [a], Onur G. Apul [a,*]

[a] Department of Civil and Environmental Engineering, University of Maine, Orono, ME, 04473, USA
[b] Senator George J. Mitchell Center for Sustainability Solutions, University of Maine, Orono, ME, 04473, USA

ARTICLE INFO

Keywords:
Adsorption
FEM
Landfill
Leachate
PFAS
Simulation

ABSTRACT

In response to growing environmental concerns regarding the presence of per- and polyfluoroalkyl substances (PFAS) in landfills, this study explores PFAS permeation through pinhole defects of high-density polyethylene (HDPE) geomembranes (GMs) experimentally. Specifically, this study aims to: (*i*) investigate the adsorption of PFAS onto HDPE GMs, (*ii*) evaluate the effectiveness of GMs experimentally in retaining PFAS-laden leachate in the event of a puncture failure, (*iii*) assess the critical conditions leading to puncture failure of GM using mechanical characterization testing with complementary finite element method (FEM) analyses with the input data from mechanical characterization. Our findings show limited intermolecular attractive interactions between PFAS and GMs, and surfactant properties of PFAS contribute to higher leachate permeation through pinholes. In general, highly fluorinated, short chain PFAS exhibit increased permeation rates, which was attributed to their size and greater propensity to align at the water-air interface. This study underlines the environmental implications of PFAS-laden leachates especially when there are no proper liner systems or leachate collection systems in place underscoring the necessity for modern landfill design and management practices to mitigate environmental risks associated with PFAS.

1. Introduction

Municipal solid waste landfills (MSWLF) are engineered sanitation facilities designed to protect environmental and public health by containing solid waste indefinitely (U.S. EPA, 2012). During the storage of waste, leachate is formed either by mechanical, chemical, and biological degradation of waste or due to infiltration of precipitation in landfills. Proper management of leachate is essential to human health and environmental sustainability because of high concentrations of known and emerging contaminants (*e.g.*, PFAS) that may otherwise outflow into the natural environment. For this, complex landfill liner systems are used in MSWLFs with several layers of barriers having low permeabilities. Typical components of liner systems are polymeric geomembranes (GM), geosynthetic clay layers, and compacted clay layers. Above these layers generally lie an integrated leachate collection system where leachate is contained and collected (see Fig. S1 in Supporting Information for the liner system cross-sectional cutout of Juniper Ridge Landfill in Maine) (Sharma et al., 2004). In this study, we focus on polymeric GMs that are defined as 1.5–5.0 mm thick sheets that are welded to each other to create a continuous layer beneath the solid waste as they are usually resistant to thermal, chemical, oxidative deterioration (Sharma et al., 2004). As a key component of landfill liner systems, GMs embrace the weight of the waste, and serve as a barrier to encounter leachate. Thus, GM integrity is one of the key determinants of whether leachate can infiltrate into the subsequent layers and eventually reach the natural environment.

High-density polyethylene (HDPE) is the most common polymer used in the manufacturing of GMs (Hsuan et al., 1998). Undamaged HDPE GMs typically have a permeability coefficient of less than 10^{-14} cm s^{-1}, which is often dubbed impermeable and offers leak protection (Xue et al., 2013a). However, the prolonged service time span of GMs in a landfill with various kinds of mechanical stresses acting on them (*e.g.*,

☆ This paper has been recommended for acceptance by Dr Jiayin Dai.

* Corresponding author.
E-mail address: onur.apul@maine.edu (O.G. Apul).

https://doi.org/10.1016/j.envpol.2024.125234
Received 12 September 2024; Received in revised form 28 October 2024; Accepted 1 November 2024
Available online 1 November 2024

construction operations that take place on top of them, thermal expansion particularly due to temperature fluctuations causing material stress and resulting in wrinkles, and poorly assessed welding points) increase their chances of puncture failure. A former investigation of a 25-year-old MSWLF revealed evidence of small holes (*i.e.*, size not reported but described as small circular defect which allows passage of light) in the GM indicating puncture failures take place (Gallagher et al., 2016). This raises a concern regarding proper sealing of GMs as a barrier since per- and polyfluoroalkyl substances (PFAS)-laden leachate has been causing apprehensions (Wei et al., 2019; Fenton et al., 2021). Specifically, research focus is required in evaluation of GMs' performance in terms of PFAS-laden leachate containment, PFAS interactions with the HDPE GMs, and elucidation of the underlying factors governing their structural integrity throughout their service life.

Perfluorooctanoic acid (PFOA) and perfluorooctane sulfonic acid (PFOS) are predominantly analyzed and reported in leachate samples (Perkola and Sainio, 2013). The average concentrations of PFOA and PFOS in landfill leachate are 1887 and 304 ng L^{-1}, respectively in the United States. The reported concentrations of PFOA range from 30 to 9200 ng L^{-1}, while for PFOS, they range from 14 to 1000 ng L^{-1} (Allred et al., 2014; Lang et al., 2017; Huset et al., 2011; Solo-Gabriele et al., 2020). Additional data on other countries are presented in the Supplementary Information section, Fig. S2. In addition, more than 60 PFAS have also been detected in leachates including perfluorobutanoic acid (PFBA), perfluorobutane sulfonate (PFBS), perfluorononanoic acid (PFNA), perfluorodecanoic acid (PFDA), perfluorohexanoic acid (PFHxA), and perfluoroheptanoic acid (PFHpA) (Zhang et al., 2023). As a consequence, 563–638 kg of PFAS is estimated to be transported to wastewater treatment plants from landfill leachates annually across the U.S. based on data from 95 landfill leachates (Lang et al., 2017). There are other estimates that show lower levels of PFAS flux in leachate as 8.5–25 kg $year^{-1}$ sent to wastewater treatment (Benskin et al., 2012). Despite the variations in the estimations, PFAS is often found in leachate and analysis of leachate-impacted groundwater from 20 historic landfills in Ontario, Canada revealed persistent PFAS contamination with concentrations as high as 12.7 μg L^{-1} (Propp et al., 2021) indicating the possibility of PFAS leakages even from engineered facilities. These findings highlight the importance of leachate collection for PFAS management. The potential permeation of PFAS-laden leachate through GMs with puncture failure is mostly unknown (Gates et al., 2020; Cerlanek et al., 2024). This study presents a novel approach by integrating bench scale testing and analytical modeling to evaluate the PFAS permeation Fig. S3. Specifically, a finite element model for puncture resistance of GM is coupled with bench-scale analysis of long term PFAS permeation, and mechanical GM properties to highlight the potential PFAS release risks associated with GM puncture failures. Specific objectives of the study are to: (*i*) investigate the adsorption of PFAS onto HDPE GMs, (*ii*) evaluate the effectiveness of GMs experimentally in retaining PFAS-laden leachate in the event of a puncture failure, (*iii*) assess the critical conditions leading to puncture failure of GM using a combined approach of mechanical characterization testing with complementary finite element method (FEM) analyses with the input data obtained from mechanical characterization.

2. Materials and methods

2.1. Geomembrane swatch sample acquisition

This study tests two HDPE GMs (*i*) textured GMs with thicknesses of 60 and 80 mil (i.e., 1.5 and 2.0 mm): and (*ii*) smooth GMs with thicknesses of 80 and 100 mil (i.e., 2.0 and 2.5 mm). HDPE was chosen as the model GM material for evaluation due to its widespread use (McWatters et al., 2016) and robustness in landfill applications (Rowe and Shoaib, 2017; Lavoie et al., 2020). Unused, textured GM swatch samples were provided by the Juniper Ridge Landfill in Old Town, Maine. The smooth GMs swatch samples were provided by Naue GmbH & Co. KG, Germany. The thicknesses of the samples were confirmed using a vernier caliper (Starrett 210AP, Athol, MA) for 60 mil, 80 mil textured and 80 mil, 100 mil smooth as 1.58 ± 0.01, 2.22 ± 0.06, 1.94 ± 0.08, and 2.57 ± 0.01 mm, respectively. The average surface roughness measurements were performed using a profilometer (Alphastep 500, Milpitas, CA) by scans at two random locations on each coupon and reported as % of the GM thickness. Geomembrane thicknesses heights for the samples were 0.16%, 0.12%, 0.02%, 0.01%, respectively.

2.2. Physicochemical characterization of geomembranes

Physicochemical properties of the GM including surface charge, hydrophobicity, crystallinity, and specific surface area were obtained to gain insight into the PFAS adsorption and leachate permeation mechanisms. The pH_{pzc} were measured using solutions of 0.1 M NaCl (Fisher Scientific, Waltham, MA) with pH values of 2, 4, 6, 8, 10, and 11. All solutions were prepared using boiled distilled and deionized (DI) water (≥18.2 MΩ-cm) to eliminate the effect of dissolved CO_2 on pH. After adjusting the pH (Corning Model 340, Corning, NY) with 0.5 M HCl and NaOH solutions (Sigma Aldrich, Saint Louis, MO), 40 mL of 0.1 M NaCl with various initial pH values were mixed with 0.2 g of HDPE GMs in sealed reactors. To reach equilibrium, the samples were placed in a horizontal shaker at a speed of 180 rpm at room temperature, and the final pH of the solution was measured after 24 h (Dastgheib et al., 2004).

Crystallinity was measured via differential scanning calorimetry (Discovery DSC Model 2500, New Castle, DE). Samples of 5–7 mg were placed into crucibles made of Al, and they were subjected to heating and cooling at a rate of 10 °C min^{-1} in a N_2 atmosphere. To completely melt the GMs, samples were first heated to 200 °C to eliminate the thermal history of the material, then cooled down to 30 °C to obtain a crystallization process curve, and again heated to 200 °C to obtain a melting curve using TRIOS analysis software (Zhou et al., 2019; Aggarwal et al., 2008). The contact angle of a droplet was detected using a Theta Optical Tensiometer (Biolin Scientific, Paramus, NJ).

The specific surface area analysis for HDPE was conducted using Kr as the probe adsorbate. The surface area measurement of the samples was carried out using Micromeritics ASAP 2020 (Norcross, GA, USA) in a liquid nitrogen environment at 77 K and the samples were degassed in N_2 at 70 °C for 8 h (Makowski et al., 2019). The Brunauer-Emmett-Teller (BET) model was used to estimate the surface area of GMs.

2.3. Mechanical characterization of geomembranes

The sealing performance of HDPE GMs are investigated by their mechanical properties, such as puncture resistance, tensile strength, and tear resistance (Xue et al., 2013b). Puncture resistance is a key property of GM integrity in landfill applications, as GMs can be prone to damage by sharp objects. The experiment was performed using an Instron 8871 machine (Instron, Norwood, MA), following the ASTM D4833 standard, with a strain rate of 300 mm min^{-1} and 10 replicates were analyzed for statistical robustness (Fig. S4 in SI) (ASTM, 2013). To evaluate the tensile strength of polymeric sheet materials, which is the ability of a material to resist a pulling force, ASTM D6693 (Type IV) tests were carried out using an Instron 5900R machine (Instron, Norwood, MA) at a strain rate of 50 mm min^{-1} (ASTM, 2010). Ten dumbbell-shaped specimens for each GM were tested in both machine and cross-machine direction (Fig. S5 in SI) (Abdelaal et al., 2015). Both tear and tensile resistance are evaluated by applying tensile forces to the samples, the point of failure for tear resistance is dictated by a specific pressure point. The tear resistance tests were carried out using the same Instron 5900R machine, following the ASTM D1004 standard, with a strain rate of 50 mm min^{-1}. Ten samples were tested in machine direction and ten samples were tested in the cross-machine direction for statistical robustness (Fig. S6 in SI) (ASTM D1004, 2013).

Furthermore, to investigate the distinction between the textured and smooth surface classes of samples, scanning electron microscopy (SEM)

was conducted on four GM samples using FEI Quanta 650,209 ESEM/EDX (FEI, Hillsboro, OR) and Zeiss NVision 40 FIB/SEM with EDAX (ZEISS, Oberkochen, Germany). For the control samples, a small coupon of GM was subjected to liquid N_2 to make it brittle and facilitate cutting. After removal from the liquid N_2 the coupons were sliced into two parts with a razor, enabling observation of the cross-section through SEM images.

2.4. Determination of leakage through geomembranes

Movement of leachate through GMs was evaluated using: (*i*) centrifuge tests with scaling principle and (*ii*) static benchtop permeation tests. Both methods tested the passage of DI water and synthetic leachate through HDPE GMs (Fig. S7 in SI). The formulation of the synthetic leachate can be found in Table S1 in the SI section. For the centrifuge testing, a Beckman Coulter centrifuge (Model Allegra 6 KR, Brea, CA) with a rotating diameter of 11 cm was employed. Centrifugal force is used to simulate a level of physical stress on the GM in the lab (*i.e.*, the model, *m*) as the field GM (*i.e.*, the prototype, *p*) would experience over the years (Shu et al., 2018). Centrifugal force, time of centrifugation, and model dimensions were determined by the same scaling ratio (*n*) (Shu et al., 2018). The model dimensions have been established by using the scaling ratios, where the prototype height (H_p) to model height (H_m) is defined as $n = \frac{H_p}{H_m}$, and the prototype time (t_p) to equivalent model time (t_m) is defined as $n = (\frac{t_p}{t_m})^{0.5}$ (Ng, 2014).

In centrifugal testing, the GM swatches were attached with high strength structural adhesive (J-B Weld, Sulphur Springs, TX) in 50 mL polypropylene centrifuge tubes with 25 mm diameter openings. The centrifuge tube was filled with 30 mm liquid height and the experiment operated at 492 g for 32–65 min to determine whether water could pass through an intact HDPE GM in 15–30 years of prototype operational equivalence. No leakage was detected.

For static benchtop leakage tests, GMs were punctured using needles with outer diameters of 0.25, 0.51, and 0.70 mm, creating a pinhole to GM swatch surface area ratio within 0.02%–0.60%. Synthetic leachate and DI water were used as test solutions (Hrapovic et al., 2002). In addition, 500 μg L^{-1} of 15 different PFAS (See Table S2 in SI) as single solute and mixtures were spiked in both solutions to see the effect of PFAS on leakage rates. The PFAS used in this study were obtained from Fisher Scientific (Waltham, MA), Sigma-Aldrich (Saint Louis, MO), SynQuest laboratories (Alachua, FL), and Apollo Scientific (Cheshire, UK). The graduated centrifuge vials were set upright on the lab benchtop and the volumetric flow rates were determined by observing the movement of 20 mL solutions through the perforated GM using a video recorded in 4K resolution at 60 frames s^{-1}. The permeation rate was recorded by measuring water volumes at 5 s intervals from the recording. The flow rates (Q) of the solutions are reported as volume m^3 s^{-1}.

The permeation of leachate under various pH, temperature, and ionic strength conditions were examined to understand the effect of PFAS on permeation rates from GMs in environmentally pertinent scenarios. The pH of samples were adjusted for acidic and basic conditions using 0.5 M HCl and NaOH, respectively, and measured with a pH meter (Corning Model 340, Corning, NY). The ionic strength was adjusted by 0.01, 0.1, and 1M KCl (Sigma Aldrich, Saint Louis, MO), and measured with a conductivity sensor (YSI, MultiLab 4010-3W, OH). The temperatures of the samples were controlled by equilibrating the experimental setup in an incubator (Fisher Scientific, Waltham, MA) for 1 h.

2.5. Adsorption of PFAS by HDPE geomembranes

The intermolecular interactions between GMs and PFAS molecules may influence the retention of PFAS during the infiltration of leachate through GM. Thus, single solute, adsorption experiments were performed using 12 g of GM liner in 1 L polypropylene containers (VWR, Radnor, PA) filled with 500 μg L^{-1} of PFOA, PFOS, PFBA, and PFBS in DI water. All bottles were shaken in a horizontal shaker at 180 rpm for 1, 2, 6, 16, 24, 48, 72, and 120 h. A control sample containing 500 μg L^{-1} of PFAS and 1 L of DI water was also tested to ensure that the concentration of PFAS was not reduced due to adsorption onto the container. The residual concentrations were then measured using Agilent 6540 Q-TOF liquid chromatography-mass spectrometry (LC/MS-MS) and an Agilent Eclipse XDB-C18 (3.5 μm, 2.1 × 100 mm) (Agilent Technologies, Santa Clara, CA). Mobile phase A consisted of DI water and 5 mM ammonium formate. Mobile phase B contained 5 mM ammonium formate in methanol. The system received 5 μL of samples using a gradient elution (B) of 0–9 min 35–80%, 9–10 min 80–95%, 10–11 min 95-35%, and 11–12 min 35%. To identify the peaks in mass spectra, N_2 gas nebulization was adjusted to 40 psi with a dry gas flow of 8 L min^{-1} at 300 °C while the sheath gas setting was adjusted to 10 L min^{-1} at 325 °C. In addition, a 3500 V capillary voltage and a 1000 V nozzle voltage were set and a mass scan ranging from m/z 100 to 1100 was performed.

A parallel set of adsorption experiments was performed using a polycyclic aromatic hydrocarbon that is frequently detected in aquatic ecosystems, phenanthrene (PNT), to test if HDPE has any adsorption capacity for other organic contaminants. The chemical was purchased from Alfa Aesar (Ward Hill, MA). Phenanthrene, an EPA designated priority pollutant, was chosen due to its similar K_{ow} value to the PFAS. A stock solution of PNT with a concentration of 500 mg L^{-1} was prepared through dissolution of a predetermined quantity of PNT in methanol (VWR, Radnor, PA). An HDPE GM swatch of 0.2 g was placed into a 40 mL glass vial. The vials were then filled completely with DI water and a specific volume of the prepared PNT stock solution was added to achieve an initial concentration of 500 μg L^{-1}. The volumetric proportion of methanol to DI water in each solution was kept below 0.1% to minimize any potential effect of cosolvents. A control sample containing 500 μg L^{-1} of PNT in a 40 mL glass vial filled with DI water was prepared to ensure PNT did not adsorb onto the container. All vials were subsequently placed on a horizontal shaker for 1, 2, 4, 6, 12, 24, 48, and 72 h to study bottle point kinetic adsorption. The PNT concentrations were measured using a UV–visible spectrophotometer (Hach DR6000, Loveland, CO) at $\lambda = 250$ nm, the maximum absorption wavelength for PNT.

2.6. Modeling the puncture failure behavior of geomembranes

Modeling the interactions between MSW and GMs is a complex problem that requires evaluating the geometrical distribution of waste particles (*i.e.*, waste fabric) and how they move relative to each other (*i.e.*, fabric evolution) to cause puncture failure (Feng et al., 2018). Given the complexity of modeling particulate behavior in MSW, a simplified model simulated potential punctures in a round swatch of GM liner. The model consists of flexible GM resting on uniformly distributed springs that simulate the stiffness of the clay layer. A uniformly distributed load simulates the weight of the MSW, and fixed pin boundary conditions simulate an interlocked sharp object in the waste. This simplification eliminates the need for complex waste fabric evolution over time by assuming that the sharp object will always protrude and carry an important reaction force within the system. The model is solved using FEM incorporating the plastic behavior of the membrane using a modified von Mises constitutive model. The derivation of the governing equation, FEM discretization, calculation cycle, computational verification, model validation, and constitutive model calibrations are detailed in *Text S1- S5* of the SI section.

3. Results and discussion

3.1. Leachate permeation through intact and punctured geomembranes

Reliability of GMs in terms of containing leachate for decades in a MSWLF is difficult to monitor because of practical limitations. Giroud and Bonaparte (1989) suggests a frequency of one hole per acre of

landfill in case of good quality assurance scenarios. However, if quality assurance measures deteriorate, the frequency can go up to ten holes per acre. According to the permeation experiments with scaling principle, all four undamaged GMs (*i.e.*, 1.5 mm textured, 2.0 mm textured, 2.0 mm smooth and 2.5 mm smooth) were able to retain liquid head of 15 m for 30 years equivalence as tested with DI water and synthetic leachate. The centrifuge experiments also indicated that any of the punctured GMs were not able to hold the DI water or leachate solution above the GM for more than 150 s, which was the shortest possible testing duration. Thus, the actual complete leakage duration could be shorter. However, it should be noted that in an actual landfill, above and below the GM layer depends on how the liner system is constructed and may change the infiltration rates. This study reveals actual permeation rates through various sizes and numbers of pinholes in a simplified experimental setup.

The open system static benchtop leakage tests found that leakage rates varied with pinhole size, number of pinholes, GM surface class, and solution type. Leakage rates were primarily governed by the size of the pinhole, with less influence from the GM surface characteristics and solution type. If the hole diameter exceeds 100 mm, GM will no longer be regarded as a barrier for liquids (Sharma et al., 2004). The ratio of the hole surface area to the overall GM surface area, which is 0.031 cm^2 per acre of landfill, is maintained in proportion to the conditions tested in our experimental setups (Giroud and Bonaparte, 1989). The data presented in Fig. 1 demonstrates an increase in the permeation rate as the number and size of the pinholes increase. Considering a round shape pinhole for the simplicity of the model, by enlarging the pinhole diameter from 0.25 mm to 0.70 mm (an increase of 685% in pinhole surface area), the permeation rate of DI water increased by approximately 500% on average for both smooth and textured GM. Furthermore, when the number of 0.70 mm diameter pinholes was increased from 1 to 5, the permeation rate of DI water exhibited an average increase of 460% for both smooth and textured GM. While conducting the experiments, we observed the flow rate was not continuous after some time for the small pinholes (*i.e.*, 0.25 mm and 0.51 mm diameter) causing flow to stop in some samples. This was attributed to the formation of small bubbles on the pinhole, or it could be influenced by the surface tension of the water, or a reduction in headwater and corresponding pressure. Given this, the combined surface area of small pinholes had less influence on leakage rates than the diameter of larger pinholes.

The surface classification of GM did not exhibit a consistent pattern across 24 duplicate permeation tests, as demonstrated in Fig. S8 in SI. However, the leachate leakage rate through textured GM significantly increased through 0.25 and 0.51 mm diameter pinholes, by 111% and 68% respectively, ($p < 0.05$). The textured GM surface may disrupt the surface tension of the solutions allowing more leachate through the pinholes especially when the pinhole diameters are small. Similarly, surface tension appears to have less influence on leakage through large pinholes than gravitational forces.

Next, permeation tests were conducted with PFAS solutions in both DI water and the synthetic leachate to evaluate the effect of PFAS on permeation. A pinhole with a diameter of 0.7 mm was selected for this experiment due to its ability to maintain a consistent flow. Additionally, this diameter ensures that the GM surface class will not interfere with the permeation rate of DI water (0.75 ± 0.01 cm^3 s^{-1}). Fig. 2a presents the rate of permeation for DI and synthetic leachate spiked with 500 μg L^{-1} PFOA and PFOS (see Figure S9 for the other types of PFAS) resulting in an increase in the permeation rate by up to 11% ($p < 0.05$) for PFOS and PFOA in DI water. Furthermore, the DI water curve in Fig. 2b exhibits the slowest rate (2.5% s^{-1}), further confirming the impact of PFAS on leakage acceleration. The results were consistently indicating that the addition of PFAS led to an increase of 10, 11, 13, and 15% in the flow rate for all tested conditions including DI water with long chain PFOS, and PFOA, and short chain PFBA, and PFBS, respectively. This enhancement was attributed to the surfactant properties of PFAS (Kancharla et al., 2022), causing a reduction of solution's surface tension. In general, short chain PFAS increased permeation rates more than long chain PFAS. The increase in permeation of PFAS-spiked leachate was statistically less significant, which can be attributed to the complexity of the solution chemistry (*vs.* DI water) and decreasing the relative impact of PFAS on surface tension due to existing surface-active compounds in synthetic leachate. To further investigate the influence of various PFAS on permeation rates, we conducted additional static benchtop experiments incorporating 11 PFAS compounds, as detailed in

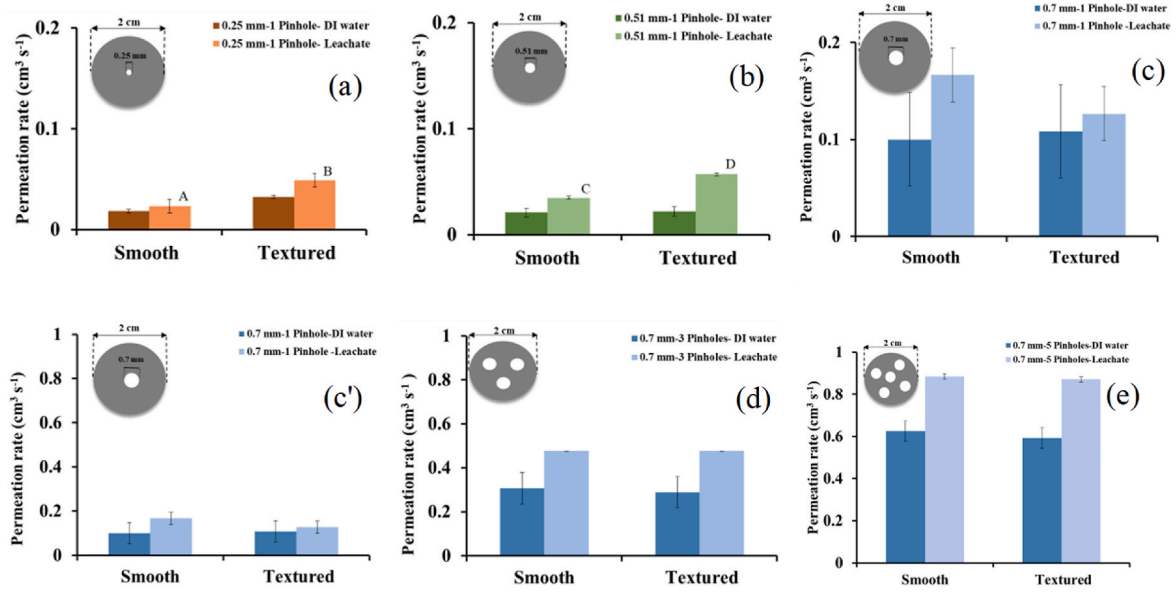

Fig. 1. Comparison of leakage rates of DI water and synthetic leachate through smooth and textured HDPE geomembranes with varying pinhole sizes and numbers. (a) a single pinhole with a diameter of 0.25 mm and pinhole ratio of 0.016%, A and B are significantly different (b) a single pinhole with a diameter of 0.51 mm and pinhole ratio of 0.064%, C and D are significantly different (c, c') a single pinhole with a diameter of 0.7 mm and pinhole ratio of 0.12%, presenting same data but differing in visualization by the y-axis for the comparison (d) 3 pinholes with diameters of 0.7 mm and pinhole ratio of 0.36% (e) 5 pinholes with diameters of 0.7 mm and pinhole ratio of 0.6%.

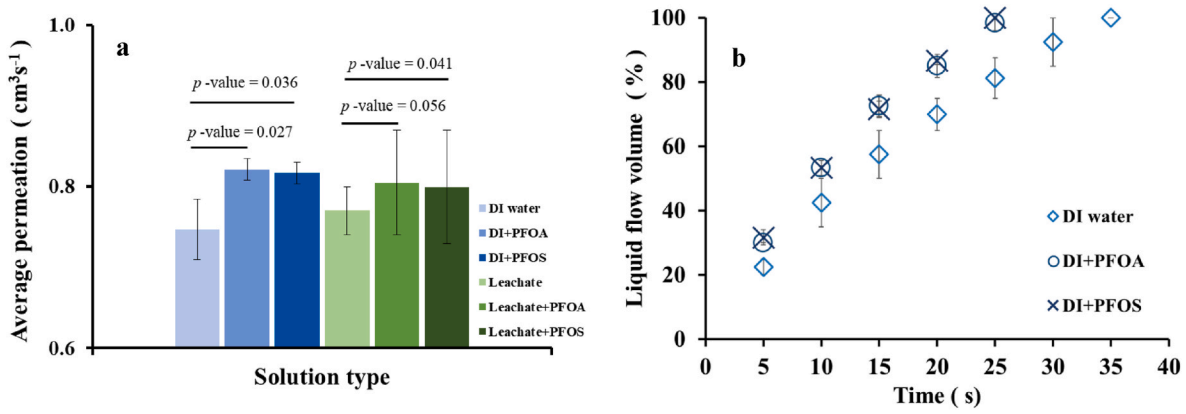

Fig. 2. (a) PFAS permeation through five 0.7 mm diameter pinholes in smooth HDPE geomembranes. (b) kinetics of PFAS permeation over a period of 5 s intervals, showing the percentage of the sample that permeates through the membrane. Error bars indicate one standard deviation for triplicate experiments.

Table S2of the Supplementary Information. The experimental outcomes demonstrated that all tested PFAS facilitate an increase in permeation rates ranging from 9 to 20% ($p < 0.05$). Notably, short chain PFAS with a higher degree of fluorination exhibit permeation rates that were 2–4% greater than those of short chain PFAS with an equivalent number of carbon atoms but lower fluorination levels. This effect can be attributed to the ability of highly fluorinated PFAS to disrupt hydrogen bonding among water molecules on the surface, thereby reducing surface tension more significantly than their less fluorinated counterparts.

Thus, PFAS can increase the permeation rate upon contact with a pinhole. As the hole size increases, the water-holding capacity of the hole decreases, and eventually the type of solution shows no effect on the permeation rate. However, realistic scenarios highlight formation of a small pinhole of 0.031 cm^2 or a large hole of 1 cm^2 per acre accounting for 7.6 $\times$ 10^{-8} and 2.5 $\times$ 10^{-6} % of the GM (Giroud and Bonaparte, 1989). Our results concluded that PFAS increased the permeation rate of leachate through pinholes but to gain a more comprehensive understanding, additional studies can be conducted for a wider range of hole diameters with variable leachate head resembling operational leachate head (*e.g.*, 0.3 m) in MWSLFs (Stark et al., 2007).

Lastly, adsorption experiments were conducted to observe if PFAS will adsorb to the GM and change the retention via intermolecular interactions. The adsorption kinetics shown in Fig. 3 (and Fig. S10 in SI) demonstrate the absence of PFOA, PFOS, PFBA, or PFBS adsorption by smooth or textured GM. Our control experiments with an aromatic polycyclic hydrocarbon (i.e., PNT, log K_{ow} = 4.48) (Crunkilton et al., 1997) with similar K_{ow} values indicated that organic compounds could adsorb onto GM and reach pseudo-equilibrium within 3 d. The hydrophobic interactions as well as nonspecific London dispersion forces may be responsible for adsorption of PNT onto GM. The smooth GM had a contact angle of 91°, which indicates a hydrophobic surface (Verdurmen-Noel et al., 2001). While, the textured GM had an average contact angle of 42°, indicating less hydrophobic behavior, which may be an analytical artifact of its rough surface because the adsorption data for PNT showed no difference between smooth vs. textured GM (Fig. S11 in SI).

In contrast, PFAS with hydrophilic and polar functional groups that are charged at ambient pH conditions could make them more likely to associate with water rather than the GM surface. The electrostatic interactions between molecules and GM, on the other hand, were found to be negligible. Our pH_{PZC} findings demonstrate (Fig. S12 in SI) that HDPE GM has no surface charge, instead it has the same pH as its surroundings and will not impact the pH of the solution. Lastly, as demonstrated in Table S3 in SI, HDPE exhibits a crystallinity level of approximately 47–49%. This characterizes HDPE as a semi-crystalline polymer, possessing a limited number of pores and reduced active surface area for adsorption purposes (Zafari et al., 2023). This is further supported by the BET analysis, which revealed a non-porous nature of HDPE and a low specific surface area that could limit its adsorption capacity. The surface area of three of four GM samples is below the detection limit (*i.e.*, 0.01 m^2 g^{-1}) (Table S4 in SI). Hence, PFAS is not expected to adsorb onto HDPE GMs and it is plausible that in the event of GM failure, PFAS would be able to leak through the GM without adsorbing onto it. Punctures in GM liners remain as a vulnerability for PFAS leakage, and its mechanical properties play a key role in its mechanical integrity.

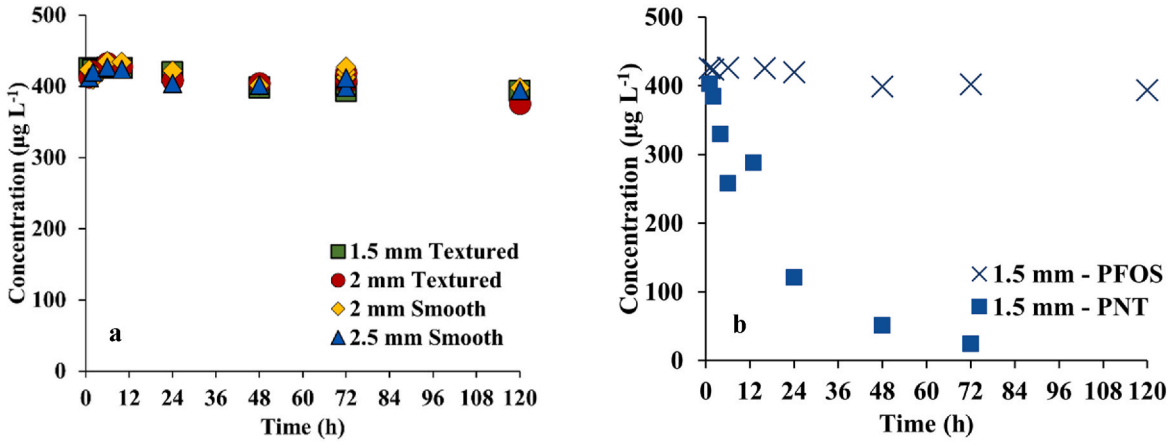

Fig. 3. (a) PFOS adsorption kinetics onto different four HDPE geomembranes. (b) PNT and PFOS adsorption kinetics on 1.5 mm HDPE geomembranes.

3.2. Effect of environmental conditions and solution chemistry on permeation through geomembranes

Fig. 4 shows the effect of pH, temperature, and ionic strength where

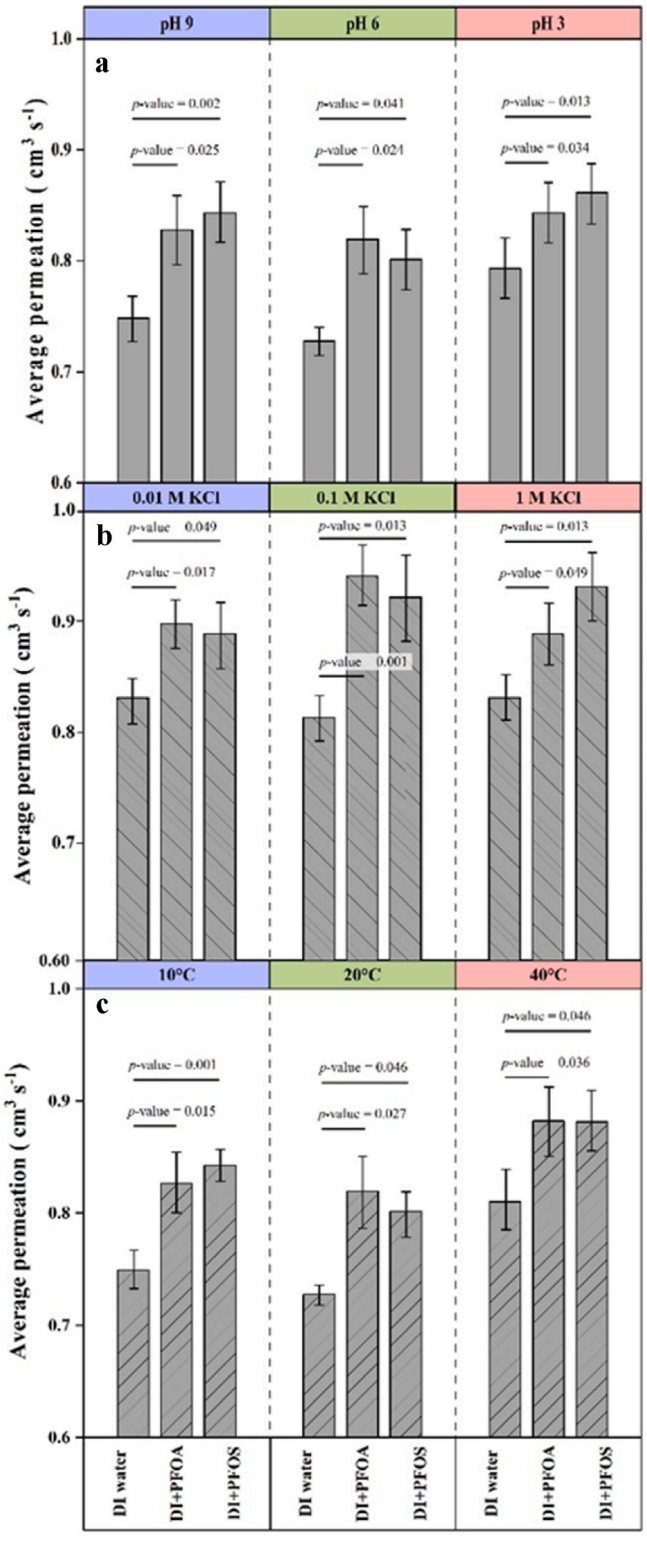

Fig. 4. The effect of different pH levels (a), ionic strengths (b), and temperatures (c) on permeation rate through five 0.7 mm pinholes in textured geomembranes. The p-values for DI water spiked with each PFAS are displayed above each column.

PFOA or PFOS significantly increased the permeation in all tested conditions by 6–15% ($p < 0.05$). The first factor tested was the solution pH (at 3, 6, and 9). Such variability is expected based on waste composition, the decomposition phase, infiltration by rainwater, (bio)chemical reactions within the landfill, management practices, and the surrounding environmental conditions (Venu et al., 2016; Wang et al., 2002; Teng et al., 2021; Stegemann et al., 2002). The decomposition of industrial and organic waste can generate acidic compounds, whereas construction materials can cause a more alkaline leachate (Zhang et al., 2016). At pH 3, there was a slight increase in permeation where more PFAS is expected to be in its acidic form *i.e.*, more hydrophobic molecules that could partition at the air-water interface. This accumulation can facilitate interaction of PFAS at the interface, and potentially lowering the surface tension. The second factor considered is the ionic strength of leachate, which can influence the permeation of PFAS by increasing ionic activity in solution (Grellier et al., 2006). The only observation of PFOS permeation was its proportional increase with ionic strength, which could be an indication of salting-out effect where higher ionic activity in solution may be causing an increase in PFOS air-water partitioning. Higher ionic strength is often found in older landfills or those containing specific types of industrial waste (Moradian et al., 2020). No other significant pattern in PFAS permeation was observed between three ionic strengths tested. The third factor evaluated was the impact of temperature on PFAS permeation (Kettunen et al., 1996; Ilies and Mavinic, 2001). At 40°C, higher permeation was observed where decreasing solution viscosity is believed to be the main factor because PFAS solubility would increase at higher temperatures, but this increase seems to be overshadowed by the decreasing solution viscosity.

Next, PFAS mixtures containing 500 ng L^{-1} short chain (PFBA + PFBS), long chain (PFOA + PFOS), a combination of short and long chain PFAS mixtures. The results indicate an increase in permeation rates for all tested conditions. However, the type and length of PFAS did not show a statistically significant difference in the permeation rates with respect to mixture types. This was attributed to the concentrations observed in leachates being too high to see an effect of PFAS mixtures. To confirm this observation, PFAS concentration down to 0.05 ng L^{-1} were tested and changes in permeation rates at ng L^{-1} levels were shown in Fig. S13.

3.3. Mechanical characterization of HDPE geomembranes

Our findings indicated that while PFAS type and solution chemistry play a role, PFAS-laden leachate permeation depends mostly on the mechanical integrity of the HDPE GMs. Since, puncture load produced by the waste material has the potential of forming pinholes, we tested the puncture resistance of GMs at various thicknesses (1.5–2.5 mm) and evaluated tensile and tear strengths to complement our understanding in material properties under stress (Sharma et al., 2004). The corresponding data of mechanic characterization for machine direction are provided in Table 1 and for cross-machine direction are Table S5 in SI.

As the thickness of GMs increases, their tensile strength, tear resistance, and puncture resistance improve, comparing maximum values of resistance presented in Table 1. The dataset indicates that smooth GMs exhibit almost twice the elongation capacity of textured GMs before reaching their breaking point under tensile loading, which aligns with the findings of Zafari et al. (Huang et al., 1994). Furthermore, the 2 mm textured GM is 2% and 10% stronger than the 2 mm smooth GM regarding the tear and puncture resistance, respectively. We conducted SEM analysis to determine whether the micro-structural arrangement of material fibers in the textured and smooth GMs contributed to the increased strength of textured GM. As shown in Fig. S14 in SI, the fibers of all GMs have become detached from the matrix material leading to the delamination of the fiber-matrix layers, a phenomenon known as fiber debonding or fiber pull-out (Wang et al., 1997). The SEM images (Fig. S14 in SI) show that the fibers of the textured samples fracture at the edges, a consequence of stress concentrations arising from uneven

Table 1
Tensile properties, tear resistance and index puncture resistance of HDPE GMs at machine direction.

Test	Method	Criteria	Unit	1.5 mm Textured	2 mm Textured	2 mm Smooth	2.5 mm Smooth
Tensile properties	ASTM 6693	Strength at yield	kN/m	26.5 ± 0.5	36.1 ± 0.5	32.4 ± 0.6	43.7 ± 1.7
		Ultimate strength	kN/m	28.8 ± 2.3	40.9 ± 3.0	67.2 ± 3.2	90.2 ± 6.6
		Strain at yield	%	17.0 ± 0.02	17.0 ± 0.01	17.0 ± 0.01	18.0 ± 0.01
		Ultimate strength	%	520 ± 0.5	576 ± 0.7	1042 ± 0.4	1016 ± 1.2
Tear resistance	ASTM D1004	Maximum Resistance	N	260 ± 2.3	355 ± 4.1	349 ± 0.8	462 ± 0.8
		Maximum Extension	mm	53.7	55.0	62.6	68.6
Index puncture resistance	ASTM D4833	Average Resistance	N	603	763	693	866

thicknesses and fiber orientation. Note that the increment of puncture strength is the most consistent value among all GMs tested. This is because the loading occurs perpendicular to the plane, producing tensile strength of the membrane in all directions. As the membrane elongates, the thickness is reduced which produces stress concentration around the loading pin and eventually an increase of shear stress on the perimeter of the pinhole that produces the puncture at smaller strains than those reported for pure tensile tests. It should be noted that small pinholes in textures GM coupons also lead to disruption of surface tension and lead to higher PFAS-laden leachate infiltration. Despite the benefits of textured GMs in terms of physical stability (higher friction between the subsequent layers), there may be some disadvantages such as mechanical vulnerability and higher PFAS permeation.

When dealing with plastic materials such as HPDE, it is more practical to plot stress-strain curves than load-elongation curves. With this, fundamental elastic parameters can be calculated and later used to calibrate the appropriate constitutive equations. In our study, we employed the tensile strength tests to calculate Young's modulus E, defined as the derivative of the tensile stress to the axial strains. We found that all GMs have a similar Young's modulus as 99.5, 108.2, 90.8, and 98.6 GPa for the 1.5 mm textured, 2.0 mm textured, 2.0 mm smooth, 2.5 mm smooth, respectively. This result reflects that all membranes are made of the same constituent material and explains that tensile strength differences are due mainly to thickness differences and microstructural composition due to differences in cross-sectional area (*i.e.*, textured vs smooth surface). Fig. S18 in SI shows the stress-strain curve for all GMs tested together with the simulated tensile strength tests simulated using the calibrated constitutive equation. The material behavior shows a peak axial strength of around 17% deformation and a subsequent rapid decrease leading to almost constant yield stress of about 14 GPa for the textured GM and 13 GPa for the smooth GM. This behavior is known as hardening-softening, and it facilitates the redistribution of stress that leads to progressive failure (Naeini et al., 2014). At around 500% deformation, a rapid hardening occurs that eventually leads to tensile failure. However, as mentioned before, puncturing failure will occur at small strains; therefore, the remarked hardening does not play any role on the mechanical response of the GMs in puncture type loading. It is worth noting that the chosen constitutive model can reproduce the peak and softening behavior of the GMs with a unique set of parameters detailed in *Text S2*.

3.4. Finite element method to investigate the vulnerability of HDPE geomembranes to puncture failure under typical landfill conditions

Experimental mechanical strength results discussed in the previous section indicated key parameters to characterize the stress-strain behavior of the HPDE GM. However, none of those tests reproduced the same initial and boundary conditions that the same GM will encounter in a typical MSWLF scenario. Thus, to complement the experimental analysis, an extensive parametric analysis was conducted to determine puncture failure comparing the maximum normalized load per unit of area of sharp object to that recorded in the puncture test. A total of sixteen cases were examined resulting from the combination of material type (smooth or textured), membrane thickness (1.5, 2.0, and 2.5 mm), waste density ($\gamma = 2.8$ and 4.2 kN/m^3), and clay liner modulus of subgrade reaction ($k_s = 30$ and 200 MN/m^3) (Qian et al., 2004). Each case consists of forty instances with an increasing sharp object diameter ranging from 1 to 20 mm in increments of 0.5 mm, resulting in a total of 640 analyses.

A sensitivity test on the parameters of the model was conducted in terms of maximum displacement of the membrane and puncture load and it is shown in Fig. S21 in SI. It is shown that the displacement measurements (*i.e.*, indentation of the GM) are more sensitive to the modulus of subgrade reaction of the clay, the membrane Poisson ratio, and landfill height with 36, 14, and 50% sensitivity respectively. In terms of puncture load, the parameters with the highest sensitivity in the model are the sharp object diameter with 93% followed by the height of the landfill with 5.7%. This is because at the predicted deformations the material has reached the yield stress, which is similar in all cases (Fig. S18 in SI). The geometrical configurations of the waste in contact with the GM (*i.e.*, height and sharp object diameter) and the properties of the clay liner (*i.e.*, modulus of subgrade reaction) control the generation of pinholes rather than the GM properties, which are predictable and uniform. It is worth noting that k_s is also an important parameter and can change based on the nature of compacted clays and their dependence on surrounding conditions such as confining pressure, thickness, and porewater pressure. However, in this work, 30 *vs.* 200 MN/m^3 range did not display a notable impact on punctual axial stress.

Puncture stresses obtained using the FEM model for all GMs are compared to the puncture strength obtained in the laboratory test in Fig. 5, where the sharp object diameters increase along the y-axis from the top to the bottom of the graph. Note that the diameter of a sharp object is inversely related to the normal puncture stress due to the enlarged surface area of contact. Because the diameter of the sharp object dominates the sensitivity of the model, the results of all 16 cases are similar. The limiting normal puncture stress is calculated from the test results summarized in Table 1 and plotted in red in Fig. 5. Points above this line indicate puncturing of the GM, and points below are safe against puncturing. According to this analysis, the threshold diameter for which the membrane will likely be punctured is 7, 6, 6, and 5 mm for the 1.5 mm textured, 2.0 mm textured, 2.0 mm smooth, 2.5 mm smooth GMs, respectively. After the sharp object penetrates the GM, lateral movements were not considered in our analysis though they may easily tear the GM, enlarging the puncture.

In summary, punctures in GMs can lead to leakage, which poses a challenge in maintaining a functional barrier between the subsurface environment and municipal solid waste leachate with PFAS or other pollutants. Despite intensive quality assurance measures, punctures in GM liners are still difficult to eliminate given the potential for installation errors, mechanical stresses, and seam deficiencies during the GM's operational lifespan (Giroud and Bonaparte, 1989). In cases where a GM is positioned between two permeable media, such as geonets or coarse gravels, the maximum leakage rate through a hole that has a greater or equal opening than the GM thickness, can be evaluated by using Bernoulli's equation, as expressed by *Equation (1)*:

$$Q = CA\sqrt{2gh_w} \quad (1)$$

Q = Flow rate (m^3 s^{-1})

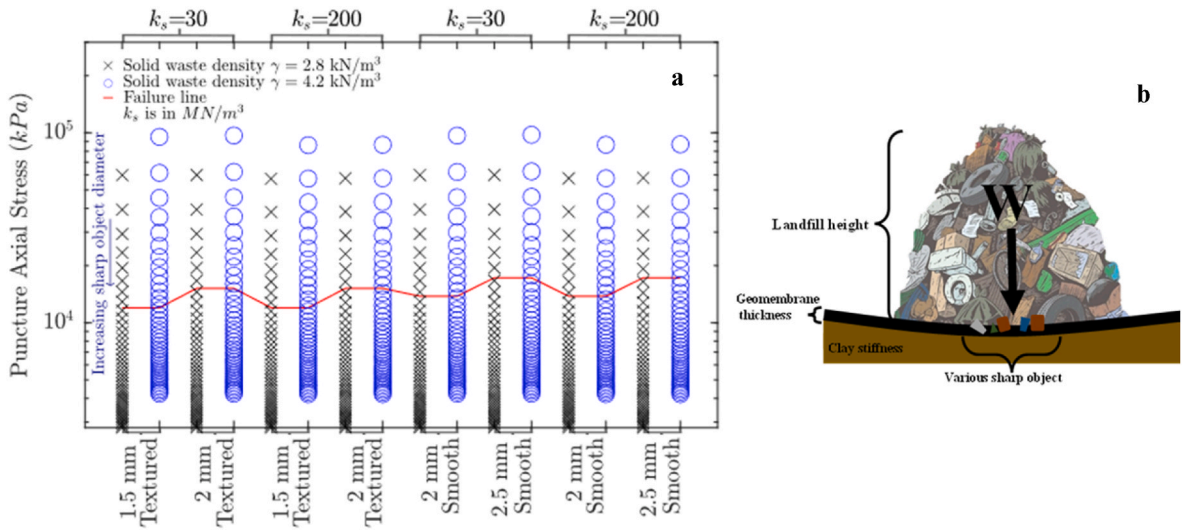

Fig. 5. (a) Puncture axial stress resulting after extensive parametric analysis using a FEM model of flexible membrane over uniformly distributed springs. The analyzed parameters include membrane surface, thickness, clay liner stiffness, waste density, and sharp object diameter. Points above the red line indicate puncture of the GM and points below are safe against puncture. (b) Conceptual model and tested independent variables used for analyzing HDPE GM puncture resistance under solid waste loads. (For interpretation of the references to color in this figure legend, the reader is referred to the Web version of this article.)

A = hole area (m^2)

C = 0.6, It is related to the shape of the sharp object (dimensionless coefficient) (Verdurmen-Noel et al., 2001)

g = acceleration due to gravity (m s^{-2})

h_w = liquid depth on top of the GM (m)

Equation (1) is valid as long as the leachate table elevation remains constant, which is an assumption if leachate is constantly drained from the landfill. The leakage rates mentioned earlier were determined under steady state, fully saturated flow conditions. Therefore, the leakage rates for 7, 6, and 5 mm holes from a GM are calculated as 5.61×10^{-5}, 4.10×10^{-5}, 2.8×10^{-5} $m^3 s^{-1}$ $acre^{-1}$. These values when complemented with the concentrations of PFAS in landfill leachate as we collect more data in time, can lead to a global estimation of PFAS escaping from the pinholes of GMs.

4. Environmental implications

There are 2636 MSWLF occupying an expansive land area of 130,482 acres in the United States (U.S. EPA). Of those, 1274 are active and they cover 91,343 acres. Under good quality assurance, with a leachate head of 0.3 m (Stark et al., 2007), and a 5.61×10^{-5} $m^3 s^{-1}$ $acre^{-1}$ flow rate, it is estimated that leakage through a 7 mm hole in a geomembrane will lead to 8 months leachate retention time in an acre of landfill. Considering that the leakage rate increases with the size of the hole, a 7 mm hole was assumed as an example average size for predicting PFAS leakage through GM in landfills in case of any defects. However, under poor quality control, the flow rate can increase by an order of magnitude, allowing the leachate to pass the GM and decrease the leachate retention time to 25-d per acre. According to the results of the PFAS adsorption study on HDPE GM, there is no affinity between PFAS and HDPE. When this is combined with the US distribution of PFAS concentrations and the poor quality assurance scenario, our calculations indicate that, on average, the amount of PFAS leakage through GM could be as high as 33.6 g (0.58–163 g) for PFOA and 5.4 g (0.25–17.5 g) for PFOS per year, per acre of landfill in the US. The sensitivity analysis conducted in this study indicates that for GM displacement and the puncture load leading to GM failure, the height of the landfill and the diameter of the sharp object are the primary influencing factors. These findings underscore the critical role of GM integrity during its installation and use in landfills, to ensure that emerging contaminants such as PFAS are effectively contained and prevented from escaping into the surrounding environment.

This study focused on GM performance in a simplified experimental setup, hence further studies are needed to investigate how subsequent liner and soil properties affect PFAS movement into soils and groundwater beneath MSWLF. Our findings indicate that the thickness of the GM and the diameter of sharp objects are significant determinants of puncture resistance, in terms of permeation. Rowe et al. (2020) underscore the importance of the selection of 2 mm HDPE GMs as they are suited for applications demanding durability and resistance to extreme chemical and thermal exposures (Rowe et al., 2020). Furthermore, research by (Dickinson et al., 2008) emphasizes the necessity of a protective layer above the GM to mitigate physical damage. They suggested a 150 mm layer of compacted clay along with another 150 mm layer of rubber tire shreds, supplemented with a nonwoven needle punctured geotextile to minimize strains (Dickinson et al., 2008). If PFAS penetrates the layer beneath the GM, the condition and integrity of subsequent layers play a crucial role in determining the fate of PFAS, indicating a need for further research. Therefore, having double composite liner systems, refining GM design and installation practices can enhance their mechanical resistance. In addition to containment strategies, there is a growing need for advanced technologies that can effectively break down and eliminate PFAS. Our study also emphasizes the critical necessity for regulatory protocols governing the design and implementation of high quality, impermeable GMs within MSWLFs as barriers against potential PFAS escape from landfills. The requirements for liner systems in MSWLs vary across jurisdictions, primarily due to the diversity of regional regulations. Therefore, improving the regulatory aspects of GMs nationwide with particular focus on proper design, operation, assessment is imperative.

CRediT authorship contribution statement

Simin Moavenzadeh Ghaznavi: Writing – original draft, Methodology, Investigation, Conceptualization. **Anthony Joshue Flores Azua:** Writing – original draft, Methodology, Investigation, Conceptualization. **A. Dianne Kopec:** Writing – review & editing, Project administration, Methodology, Conceptualization. **Luis Zambrano Cruzatty:** Writing – review & editing, Methodology, Conceptualization. **Onur G. Apul:** Writing – review & editing, Supervision, Project administration, Methodology, Funding acquisition, Conceptualization.

Declaration of competing interest

The authors declare that they have no known competing financial interests or personal relationships that could have appeared to influence the work reported in this paper.

Acknowledgements

This work received funding from NSF (2219832) and the FY22 Water Resources Sustainability Research Grants (USGS 104g; Grant Reference No. G22AP00014-00) administered by the Maine Water Resources Research Institute at the Senator George J. Mitchell Center for Sustainability Solutions at the University of Maine in Orono, Maine. The opinions presented here may not reflect the opinions of the funding agency. We would like to thank Eric Landis for his support in material characterization and Neil Fisher and Sudheera Yaparatne for their assistance in setting up the experimental setup.

Appendix A. Supplementary data

Supplementary data to this article can be found online at https://doi.org/10.1016/j.envpol.2024.125234.

Data availability

Data will be made available on request.

References

Abdelaal, F.B., Rowe, R.K., Hsuan, Y.G., Awad, R., 2015. Effect of high temperatures on the physical and mechanical properties of HDPE geomembranes in air. Geosynth. Int. 22 (3), 207–224.
Aggarwal, S., Sajwan, M., Singh, R.B., 2008. Crystallinity of hdpe pipes by dsc, xrd and ftir spectroscopy-a Forensic comparison. Indian J. Criminol. Crim 2, 141–148.
Allred, B.M., Lang, J.R., Barlaz, M.A., Field, J.A., 2014. Orthogonal zirconium diol/C18 liquid chromatography–tandem mass spectrometry analysis of poly and perfluoroalkyl substances in landfill leachate. J. Chromatogr. A 1359, 202–211.
ASTM, 2010. Standard Test Method for Determining Tensile Properties of Nonreinforced Polyethylene and Nonreinforced Flexible Polypropylene Geomembranes. D6693-04.
ASTM, 2013. Standard Test Method for Index Puncture Resistance of Geomembranes and Related Products. American Society for Testing and Materials, Philadelphia, PA, USA.
ASTM D1004, 2013. Standard Test Method for Tear Resistance (Graves Tear) of Plastic Film and Sheeting. American Society for Testing and Materials.
Benskin, J.P., Li, B., Ikonomou, M.G., Grace, J.R., Li, L.Y., 2012. Per-and polyfluoroalkyl substances in landfill leachate: patterns, time trends, and sources. Environ. Sci. Technol. 46 (21), 11532–11540.
Cerlanek, A.R., Timshina, A.S., Robey, N., Lin, A.M., Solo-Gabriele, H.M., Townsend, T. G., Bowden, J.A., 2024. Investigating the partitioning behavior of per-and polyfluoroalkyl substances (PFAS) during thermal landfill leachate evaporation. J. Hazard Mater. 472, 134500.
Crunkilton, R.L., DeVita, W.M., 1997. Determination of aqueous concentrations of polycyclic aromatic hydrocarbons (PAHs) in an urban stream. Chemosphere 35 (7), 1447–1463.
Dastgheib, S.A., Karanfil, T., Cheng, W., 2004. Tailoring activated carbons for enhanced removal of natural organic matter from natural waters. Carbon 42 (3), 547–557.
Dickinson, S., Brachman, R.W.I., 2008. Assessment of alternative protection layers for a geomembrane–geosynthetic clay liner (GM–GCL) composite liner. Can. Geotech. J. 45 (11), 1594–1610.
Feng, S.J., Liu, X., Chen, H.X., Zhao, T., 2018. Micro-mechanical analysis of geomembrane-sand interactions using DEM. Comput. Geotech. 94, 58–71.
Fenton, S.E., Ducatman, A., Boobis, A., DeWitt, J.C., Lau, C., Ng, C., Smith, J.S., Roberts, S.M., 2021. Per-and polyfluoroalkyl substance toxicity and human health review: current state of knowledge and strategies for informing future research. Environ. Toxicol. Chem. 40 (3), 606–630.
Gallagher, E.M., Tonks, D.M., Shevelan, J., Belton, A.R., Blackmore, R.E., 2016. Investigations of geomembrane integrity within a 25-year old landfill capping. Geotext. Geomembranes 44 (5), 770–780.
Gates, W.P., MacLeod, A.J., Fehervari, A., Bouazza, A., Gibbs, D., Hackney, R., Callahan, D.L., Watts, M., 2020. Interactions of per-and polyfluoralkyl substances (PFAS) with landfill liners. Advances in Environmental and Engineering Research 1 (4), 1, 1.
Giroud, J.P., Bonaparte, R., 1989. Leakage through liners constructed with geomembranes—part I. Geomembrane liners. Geotext. Geomembranes 8 (1), 27–67.
Grellier, S., Robain, H., Bellier, G., Skhiri, N., 2006. Influence of temperature on the electrical conductivity of leachate from municipal solid waste. J. Hazard Mater. 137 (1), 612–617.
Hrapovic, L., Rowe, R.K., 2002. Intrinsic degradation of volatile fatty acids in laboratory-compacted clayey soil. J. Contam. Hydrol. 58 (3–4), 221–242.
Hsuan, Y.G., Koerner, R.M., 1998. Antioxidant depletion lifetime in high density polyethylene geomembranes. J. Geotech. Geoenviron. Eng. 124 (6), 532–541.
Huang, N.C., Liu, X.Y., 1994. Debonding and fiber pull-out in reinforced composites. Theor. Appl. Fract. Mech. 21 (3), 157–176.
Huset, C.A., Barlaz, M.A., Barofsky, D.F., Field, J.A., 2011. Quantitative determination of fluorochemicals in municipal landfill leachates. Chemosphere 82 (10), 1380–1386.
Ilies, P., Mavinic, D.S., 2001. The effect of decreased ambient temperature on the biological nitrification and denitrification of a high ammonia landfill leachate. Water Res. 35 (8), 2065–2072.
Kancharla, S., Alexandridis, P., Tsianou, M., 2022. Sequestration of per-and polyfluoroalkyl substances (PFAS) by adsorption: surfactant and surface aspects. Curr. Opin. Colloid Interface Sci. 58, 101571.
Kettunen, R.H., Hoilijoki, T.H., Rintala, J.A., 1996. Anaerobic and sequential anaerobic-aerobic treatments of municipal landfill leachate at low temperatures. Bioresour. Technol. 58 (1), 31–40.
Lang, J.R., Allred, B.M., Field, J.A., Levis, J.W., Barlaz, M.A., 2017. National estimate of per-and polyfluoroalkyl substance (PFAS) release to US municipal landfill leachate. Environ. Sci. Technol. 51 (4), 2197–2205.
Lavoie, F.L., Kobelnik, M., Valentin, C.A., Silva, J.L.D., 2020. Durability of HDPE geomembranes: an overview. Quím. Nova 43, 656–667.
Makowski, T., Zhang, C., Olah, A., Piorkowska, E., Baer, E., Kregiel, D., 2019. Modification of dual-component fibrous materials with carbon nanotubes and methyltrichlorosilane. Mater. Des. 162, 219–228.
McWatters, R.S., Rutter, A., Rowe, R.K., 2016. Geomembrane applications for controlling diffusive migration of petroleum hydrocarbons in cold region environments. J. Environ. Manag. 181, 80–94.
Moradian, F., Ramavandi, B., Jaafarzadeh, N., Kouhgardi, E., 2020. Effective treatment of high-salinity landfill leachate using ultraviolet/ultrasonication/peroxymonosulfate system. Waste management 118, 591–599.
Naeini, S.A., Ziaie Moayed, R., Allahyari, F., 2014. Subgrade reaction modulus (Ks) of clayey soils based on field tests. J. Eng. Geol. 8 (1), 2045–2046, 2021.
Ng, C.W., 2014. The state-of-the-art centrifuge modelling of geotechnical problems at HKUST. J. Zhejiang Univ. - Sci. 15 (1), 1–21.
Perkola, N., Sainio, P., 2013. Survey of perfluorinated alkyl acids in Finnish effluents, storm water, landfill leachate and sludge. Environ. Sci. Pollut. Control Ser. 20 (11), 7979–7987.
Propp, V.R., De Silva, A.O., Spencer, C., Brown, S.J., Catingan, S.D., Smith, J.E., Roy, J. W., 2021. Organic contaminants of emerging concern in leachate of historic municipal landfills. Environmental Pollution 276, 116474.
Qian, X., Gray, D.H., Koerner, R.M., 2004. Estimation of maximum liquid head over landfill barriers. J. Geotech. Geoenviron. Eng. 130 (5), 488–497.
Rowe, R.K., Shoaib, M., 2017. Long-term performance of high-density polyethylene (HDPE) geomembrane seams in municipal solid waste (MSW) leachate. Can. Geotech. J. 54 (12), 1623–1636.
Rowe, R.K., Abdelaal, F.B., Zafari, M., Morsy, M.S., Priyanto, D.G., 2020. An approach to high-density polyethylene (HDPE) geomembrane selection for challenging design requirements. Can. Geotech. J. 57 (10), 1550–1565.
Sharma, H.D., Reddy, K.R., 2004. Geoenvironmental Engineering: Site Remediation, Waste Containment, and Emerging Waste Management Technologies. John Wiley & Sons.
Shu, S., Zhu, W., Wang, S., Ng, C.W.W., Chen, Y., Chiu, A.C.F., 2018. Leachate breakthrough mechanism and key pollutant indicator of municipal solid waste landfill barrier systems: centrifuge and numerical modeling approach. Sci. Total Environ. 612, 1123–1131.
Solo-Gabriele, H.M., Jones, A.S., Lindstrom, A.B., Lang, J.R., 2020. Waste type, incineration, and aeration are associated with per-and polyfluoroalkyl levels in landfill leachates. Waste management 107, 191–200.
Stark, N.M., Matuana, L.M., 2007. Characterization of weathered wood–plastic composite surfaces using FTIR spectroscopy, contact angle, and XPS. Polym. Degrad. Stabil. 92 (10), 1883–1890.
Stegemann, J.A., Buenfeld, N.R., 2002. Prediction of leachate pH for cement paste containing pure metal compounds. J. Hazard Mater. 90 (2), 169–188.
Teng, C., Zhou, K., Peng, C., Chen, W., 2021. Characterization and treatment of landfill leachate: a review. Water Res. 203, 117525.
U.S. EPA. Landfill Methane Outreach Program (LMOP, July 2023 https://www.epa.gov/lmop/landfill-technical-data.
U.S. EPA, 2012. RCRA Subtitle D (40 CFR §258.40) Criteria for Municipal Solid Waste Landfills: Design Criteria.
Venu, D., Gandhimathi, R., Nidheesh, P.V., Ramesh, S.T., 2016. Effect of solution pH on leachate treatment mechanism of peroxicoagulation process. Journal of Hazardous, Toxic, and Radioactive Waste 20 (3), 06016001.
Verdurmen-Noel, L., Baldo, L., Bremmers, S., 2001. SEC–FTIR characterization of semi-crystalline HDPE and PP. Polymer 42 (13), 5523–5529.
Wang, W.M., Sluys, L.J., De Borst, R., 1997. Viscoplasticity for instabilities due to strain softening and strain-rate softening. Int. J. Numer. Methods Eng. 40 (20), 3839–3864.
Wang, Z.P., Zhang, Z., Lin, Y.J., Deng, N.S., Tao, T., Zhuo, K., 2002. Landfill leachate treatment by a coagulation–photooxidation process. J. Hazard Mater. 95 (1–2), 153–159.
Wei, Z., Xu, T., Zhao, D., 2019. Treatment of per-and polyfluoroalkyl substances in landfill leachate: status, chemistry and prospects. Environ. Sci. J. Integr. Environ. Res.: Water Research & Technology 5 (11), 1814–1835.
Xue, Q., Zhang, Q., Li, Z.Z., Xiao, K., 2013a. The tension and puncture properties of HDPE geomembrane under the corrosion of leachate. Materials 6 (9), 4109–4121.

Xue, Q., Zhang, Q., Li, Z.Z., Xiao, K., 2013b. The tension and puncture properties of HDPE geomembrane under the corrosion of leachate. Materials 6 (9), 4109–4121.
Zafari, M., Abdelaal, F.B., Rowe, R.K., 2023. Degradation behavior of two multilayered textured white HDPE geomembranes and their smooth edges. J. Geotech. Geoenviron. Eng. 149 (5), 04023020.
Zhang, Y., Cetin, B., Likos, W.J., Edil, T.B., 2016. Impacts of pH on leaching potential of elements from MSW incineration fly ash. Fuel 184, 815–825.
Zhang, M., Zhao, X., Zhao, D., Soong, T.Y., Tian, S., 2023. Poly-and perfluoroalkyl substances (PFAS) in landfills: occurrence, transformation and treatment. Waste Manag. 155, 162–178.
Zhou, L., Wang, X., Zhang, Y., Zhang, P., Li, Z., 2019. An experimental study of the crystallinity of different density polyethylenes on the breakdown characteristics and the conductance mechanism transformation under high electric field. Materials 12 (17), 2657.